BNL-108441-2015-JA

Synchrotron micro-scale measurement of metal distributions in *P. australis* and *T. latifolia* root tissue from an urban brownfield site

Huan Feng[1*], Yu Qian[1], Frank J. Gallagher[2], Weiguo Zhang[3], Lizhong Yu[3], Chang-Jun Liu[4], Keith W. Jones[4], Ryan Tappero[5]

1. Department of Earth and Environmental Studies, Montclair State University, Montclair, New Jersey 07043, USA
2. Urban Forestry Program, Department of Ecology, Evolution and Natural Resources, Rutgers, The State University of New Jersey, New Brunswick, New Jersey 08901, USA
3. State Key Laboratory of Estuarine and Coastal Research, East China Normal University, Shanghai 200062, PRC
4. Biological, Environmental and Climate Sciences Department, Brookhaven National Laboratory, Upton, New York 11973, USA
5. Photon Sciences Directorate, Brookhaven National Laboratory, Upton, New York 11973, USA

* Corresponding author.

E-mail address: fengh@mail.montclair.edu; Tel: 1-973-655-7549; Fax: 1-973-655-4072.

Abstract:

Liberty State Park in New Jersey, USA, is a "brownfield" site containing various levels of contaminants. To investigate metal uptake and distributions in plants on the brownfield site, *Phragmites australis* and *Typha latifolia* were collected in Liberty State Park during the growing

season (May – September) in 2011at two sites with the high and low metal loads, respectively. The objective of this study was to understand the metal (Fe, Mn, Cu, Pb and Zn) concentration and spatial distributions in *Phragmites australis* and *Typha latifolia* root systems with micro-meter scale resolution using synchrotron X-ray microfluorescence (μXRF) and synchrotron X-ray computed microtomography (μCMT) techniques. The root structure measurement by synchrotron μCMT showed that high X-ray attenuation substance appeared in the epidermis. Synchrotron μXRF measurement showed that metal concentrations and distributions in the root cross-section between epidermis and vascular tissue were statistically different. Significant correlations were found between metals (Cu, Mn, Pb and Zn) and Fe in the epidermis, implying that metals were scavenged by Fe oxides. The results from this study suggest that the expression of metal transport and accumulation within the root systems may be element specific. The information derived from this study can improve our current knowledge of the wetland plant ecological function in brownfield remediation.

Keywords: *Phragmites australis*; *Typha latifolia*; trace metals; synchrotron radiation technique; brownfield

Introduction

Numerous studies have shown that soils/sediments in urban-industrial areas often contain mixed organic and inorganic contaminants (e.g., Feng et al., 1998, 2004; Zhang et al., 2009). "Brownfields", which are abandoned industrial land, have presented environmental concerns for decades because one of the most pressing issues caused by "brownfield" is the presence of

anthropogenic metal contamination (Gallagher et al., 2008; Koelmel and Amarasiriwardena, 2012). Restoration of "brownfield" sites with green technologies is a challenge (Feng et al., 2005; Weis and Weis, 2004). It is reported that plants can uptake metals from the contaminated soils through roots, translocate the metals to stems and leaves and accumulate these metals within the plant tissues (Lacerda et al., 1997; Qian et al., 2012; Rascio and Navari-Izzo, 2011; Williams et al., 1994). Therefore, metal distributions in the root tissue are the consequence of root metal uptake and transportation (Marschner, 2012; Merchant, 2010). Some metal ions can enter apoplast freely through root epidermis and passively diffuse through apoplast due to concentration gradient and evapotranspiration. At the same time, some metals can enter symplast through cell membranes at root epidermis under the assistance of selective transporters (Marschner, 2012; Taiz and Zeiger, 2010). Iron plaque, which is predominantly a layer of amorphous Fe hydroxide, is often observed on the surface of wetland plant root tissue. It can adsorb or co-precipitate metals due to its negative-charged surface. Iron plaque was identified as a buffer or barrier that capable of enhancing or reducing plant metal uptake efficiency (Tripathi et al., 2014). The investigation of metal uptake by plants root system and distribution in the root tissues can provide useful information of understanding the function of plants for bioremediation and phytoextraction of metals in the contaminated soils.

Liberty State Park in northern New Jersey is a brownfield site with a portion of wetland. During the 19^{th} and 20^{th} centuries Liberty State Park in New Jersey was used as a railroad yard finally closing in 1969 (Gallagher et al., 2008). Soils in the park were severely contaminated because of the original filling materials and railroad operation over a century. After conducted corrective actions, such as clean soil capping and asphalt isolation, most part of the park was reopened to the public for recreation and was officially announced as Liberty State Park in 1976

(NJDEP, 1995; LSP, 2008). However, a 251 acre of brownfield was left unremediated in the middle of the park. Previous studies showed that soil metal concentrations in this portion of Liberty State Park exceeded both ecological and residential screening criteria (Gallagher et al., 2008; Qian et al., 2012). This site has remained isolated and much of the area has been re-colonized by various plant assemblages that represent unique associations of both endemic and nonnative species (Gallagher et al., 2008). The Liberty State Park management plans call for the restoration of approximately 44,500 m^2 (11 acres) of freshwater wetlands and the maintenance of approximately 60,700 m^2 (15 acres) of native urban wetlands (USACE, 2005). Thus, the site provides a unique laboratory for studying metal uptake and distribution in the plants as exemplified by this urban brownfield since plants acquire metals from the rhizosphere soil and regulate their uptake within the root system (Hinsinger and Courchesne, 2008; McLaughlin et al., 1998). In order to understand the important role the plants play in metal uptake, translocation and accumulation in the plants, Qian et al. (2012) used bioconcentration factor (BCF), which is defined as a ratio of metal concentrations in the plant root to that in the soil, to evaluate metal uptake efficiency by plants in Liberty State Park. They found that the metal BCF varied among the metals and plant species.

Synchrotron X-ray microbeam techniques, such as synchrotron X-ray microfluorescence (μXRF) and synchrotron X-ray computed microtomography (μCMT), have important applications in high resolution study of metal transport and distribution in plants. The unique advantages of synchrotron-based techniques with high detection sensitivity and spatial resolution measurement have led to a better understanding of metal transport and distribution in plants (Feng et al., 2013; Martin et al., 2006; Punshon et al., 2009). In this study, we applied

91 synchrotron CMT to show the root structure and XRF to map metal distributions in the wetland
92 plant root system and assess the role of Fe plaque in metal accumulation in the roots.
93
94 **1. Materials and methods**
95
96 *1.1 Study area*
97
98 Two sites in Liberty State Park, Site TP-1 and Site TP-43, were selected for this
99 investigation (Figure 1). Site TP-1 in the northwest section of the study area was reported to have
100 the lowest total soil metal load in the entire study area (Gallagher et al., 2008). The soil metal
101 concentrations at Site TP-1 were found to be 19400 μg g^{-1} for Fe, 244 μg g^{-1} for Mn, 124±51 μg
102 g^{-1} for Cu, 453±266 μg g^{-1} for Pb and 309±125 μg g^{-1} for Zn, respectively (Gallagher,
103 unpublished data; Qian et al., 2012; Qian, 2015). The dominant plant species at this site were
104 *Typha latifolia* and *Phragmites australis*. Site TP-43 was located in the southwest section of the
105 study area with relatively higher soil metal load (Gallagher et al., 2008). The site was within the
106 wetland with standing water on the site under normal climatic condition. The soil metal
107 concentrations at Site TP-43 were found to be 25400 μg g^{-1} for Fe, 312 μg g^{-1} for Mn, 166±72 μg
108 g^{-1} for Cu, 333±132 μg g^{-1} for Pb and 63.1±15.6 μg g^{-1} for Zn, respectively (Gallagher,
109 unpublished data; Qian et al., 2012; Qian, 2015). This site was classified as successional northern
110 hardwood, containing perimeter areas dominated by *Phragmites australis*.
111
112 *1.2 Sample collection and preparation*
113

Field work for the plant sample collection in Liberty State Park was conducted in May 2011 for *Typha latifolia* and *Phragmites australis* at Site TP-1 and *Phragmites australis* at Site TP-43, respectively. There found no *Typha latifolia* at Site TP-43 in May 2011. Because the synchrotron XRF analysis for *Phragmites australis* collected at Site TP-1 in May 2011 was not a success, it was collected again in September 2011. These samples were collected using stainless steel spades and placed into large plastic containers and then transported immediately to Montclair State University for further treatment. The samples were cleaned by gently shaking off bulk soil with hands and rinsing off residual soils with deionized water. Some of the fresh root samples were processed immediately for synchrotron μXRF analysis, while others were oven dried separately at 30°C for synchrotron μCMT analysis. For synchrotron μCMT analysis, a section of dry, clean root sample in a length of 2 cm was placed in a Kapton tube and put on a holding stand for the measurement. For synchrotron μXRF analysis, the fresh root samples were suspended in an optimal cutting temperature (OCT) compound that does not infiltrate the specimen, and cooled at -20°C in a cryotome chamber (Cryostat CM1950, Leica Microsystems) (Feng et al., 2013). Once OCT solidified, the cryotome was used to cut a 30 μm thin cross-section of the root sample. The thin section of the root samples were then mounted on a 25 mm × 76 mm quartz microscope slide (SPI Supplies®) and kept in a desiccator at NSLS X27A Beamline until synchrotron μXRF analysis was conducted.

1.3 Synchrotron computed microtomography (μCMT) and X-ray microfluorescence (μXRF) measurement

Three-dimensional (3D) visualization of *Typha latifolia* and *Phragmites australis* root structures was achieved using synchrotron X-ray computed microtomography (μCMT) technique at the NSLS X2B Beamline of the National Synchrotron Light Source (NSLS) at Brookhaven National Laboratory (Upton, NY) (Jones et al., 2013). The tomography apparatus used a Si (1,1,1) monochromator to produce a monoenergetic beam of 10.0 keV. A beam size of about 6 mm x 6 mm was used to irradiate the root sample contained in a Kapton tube. The beam transmitted through the sample was detected with a CsI(Tl) scintillator. Light from the scintillator was magnified and then imaged using a CCD camera with dimensions of 1340 x 1300 pixels of 4 μm size. The tomographic volume was produced from a collection of 1200 images taken in 0.15° steps. Metal (Fe, Mn, Cu, Pb and Zn) concentrations and distribution within the root tissue were investigated using synchrotron μXRF at NSLS X27A Beamline (Ablett et al., 2006). Briefly, this bend magnet beamline used Kirkpatrick-Baez (K-B) mirrors to produce a focused spot (10 μm x 10 μm) of hard X-rays with tunable energy achieved via Si(111) or Si(311) channel-cut monochromator crystals. For synchrotron μXRF imaging, the incident beam energy was fixed at 13.5 keV to excite all target elements simultaneously. The sample was oriented at 45° to the incident beam, and rastered in the path of the beam by an XY stage while X-ray fluorescence was detected by a 13-element Canberra Ge array detector positioned at 90° to the incident beam. Elemental maps were typically collected from a 1 mm^2 sample area using a step size of 10 or 20 μm and a dwell time of 7 seconds. The fluorescence yields were normalized to the changes in intensity of the X-ray beam (I_0) and the dwell time. During the measurement, the X-ray influences were comparatively low and radiation damage effects were minimal.

1.4 Data analysis

159

160 The metal concentration from synchrotron μXRF measurement was in the units of counts
161 per second (cps). It was converted to the units of $\mu g\ g^{-1}$ by calibrating the samples against the
162 NIST SRM 1832 and 1833 thin glass film on polycarbonate for x-ray fluorescence spectrometry,
163 provided the root tissue density was 1.0 $\mu g\ g^{-1}$. This calibration method did not account for
164 differences in sample matrix and assumed that the absorption correction was not necessary,
165 which works well for thin samples of uniform thickness. In data analysis, Pearson correlation
166 analysis was performed on the data to examine the relationship between the metals (Fe, Mn, Cu,
167 Pb and Zn) in the epidermis and the vascular tissue, respectively, in *Typha latifolia* and
168 *Phragmites australis* collected at the two sites. Statistical t-test analysis was performed on the
169 data to examine metal concentration differences between the epidermis and the vascular tissue of
170 each plant root. Tukey Method ($p < 0.05$) was used for multiple comparison tests. To further
171 examine the processes and mechanisms governing the metal transport and distribution, factor
172 analysis was performed on the metals (Cu, Fe, Mn, Pb and Zn) (Gotelli and Ellison 2004).
173 Logarithmic transformation was performed on the data before the analysis to ensure a normal
174 distribution. Varimax rotation was used to maximize the sum of the variance of the factor
175 coefficients (Gotelli and Ellison, 2004).

176

177 **2. Results and discussion**

178

179 *2.1 Root structure visualization and metal distributions in roots*

180

181 As shown in Figure 2, synchrotron μCMT visualization of the plant root structure shows
182 high X-ray attenuation occurring in epidermis of the root tissue. Rhizosphere is a favorable
183 environment for microbial communities that enhance the biogeochemical reactions in wetland
184 plant root system (Gilbert and Frenzel, 1998). Metal availability for plant uptake is dependent on
185 soil pH, redox potential (pE), water availability, microbes and other biota, mineral and organic
186 contents, and is complicated by synergistic interactions between these variables (e.g., Dzantor
187 and Beauchamp, 2002; Martin et al., 2003; 2006; Morrissey and Guerinot, 2009; Naftel et al.,
188 2002). However, the synchrotron μCMT measurement in this study could not identify the
189 chemical composition of the high attenuation substances (Figure 3). Metal (Cu, Fe, Mn, Pb and
190 Zn) concentrations and distributions made from synchrotron X-ray microfluorescence (μXRF)
191 measurement show differences from epidermis to vascular tissue with relatively higher
192 concentrations in the epidermis than that in the vascular tissue (Figures 4-6). High concentration
193 of Fe in the root epidermis is found and can be attributed to the formation of Fe plaque due to
194 redox reaction at the soil–root interface in rhizosphere (Hansel et al., 2001, 2002; Otte et al.,
195 1989; St-Cyr and Crowder, 1990). In the epidermis, Fe must be included in the high attenuation
196 substance shown in Figures 2 and 3, which is supported by the information from synchrotron
197 μXRF measurement that indicates high Fe concentration in the epidermis (Figures 4-6). As an Fe
198 species, it has been reported that Fe plaque in the plant roots is predominantly Fe oxides (Feng et
199 al., 2013; Hansel et al., 2001; St-Cyr and Campbell, 1996). Because other trace metals (e.g., Cu,
200 Mn, Pb and Zn) were also found in the epidermis (Figures 4-6), the results suggest that these
201 trace metals could be associated with Fe plaque or Fe-oxides and included in this high
202 attenuation substances in the epidermis due possibly to scavenge by Fe plaque.
203

204 *2.2 Metal concentration difference between epidermis and vascular tissue in roots*

205

206 In order to understand the metal transport and accumulation in the root system and, in the
207 meantime, avoid processing massive data, two subareas were selected within the plant root cross-
208 section of each species, one in the epidermis and the other in the vascular tissue as indicated in
209 the optical images shown in Figures 4-6. Each subarea contains 80 to 200 data points and
210 represents a range of metal concentrations for statistical analysis. The average concentrations of
211 metals (Cu, Fe, Mn, Pb and Zn) in each subarea in the epidermis and vascular tissue of those two
212 species, *Phragmites australis* and *Typha latifolia*, are summarized in Table 1. In general, metal
213 concentrations in the epidermis were higher than that in the vascular issue. In this study,
214 Student *t*-test was performed to examine the difference in metal (Cu, Fe, Mn, Pb and Zn)
215 concentrations between the epidermis and the vascular tissue. As shown in Table 1, the results
216 show significant differences ($p < 0.01$) in metal (Cu, Fe, Mn, Pb and Zn) concentrations between
217 the epidermis and the vascular tissue in each of the plant roots. The difference in metal
218 concentrations between the epidermis and the vascular tissue can be explained by different
219 mechanisms. In the epidermis, metal adsorption/desorption at the soil-plant root interface, metal
220 uptake and transport by the plants and metal scavenge by Fe-Mn oxides are the major controlling
221 mechanisms (Bargar et al., 1997; Feng et al., 2013; Hansel et al., 2001; Liu et al., 2004), while
222 metal accumulation in vascular tissue can be dominantly controlled by the biological (or
223 biochemical) processes such as metal symplastic or apoplastic transport in the roots (Baxter et al.,
224 2008; Lyubenova et al., 2013; MacFarlane and Burchett, 2002).

225 Previous studies at Liberty State Park, New Jersey, showed that metals could be
226 translocated from the plant roots to the aerial parts although the concentrations in above-ground

227 tissues were at least an order of magnitude lower than that in the root tissue (Gallagher et al.,
228 2008; Qian et al., 2012). Various mechanisms regulating cytoplasmic metal concentration have
229 been put forward, of which chelation and sequestration of metals by particular ligands are
230 important mechanisms used by plants to deal with metal stress (Brune et al., 1994; Palmer and
231 Guerinot, 2009). In an earlier study of plant uptake of metals in Liberty Study Park, Qian et al.
232 (2012) found that metal uptake and bioaccumulation in the plants increased with increasing soil
233 metal concentration. Low organic matter content was in favor of bioaccumulation of Cu in the
234 roots, while low pH was generally in favor of bioaccumulation of Zn in the roots (Qian et al.,
235 2012). It is known that adequate amount of metals in soils are essential nutrients for the plant
236 growth. After uptake of these metals as the nutrients, the plants translocate the metals from
237 epidermis to vascular tissue and further to stem and leaf (Gallagher et al., 2008; Qian et al.,
238 2012). However, high metal concentrations are toxic to the plants. Plants that are metal excluders
239 can restrict metal entrance based on their tolerance and even hypertolerance strategies. These
240 plants can retain and detoxify most of the toxic metals in the root tissues with a minimized
241 translocation to the leaves (Deng et al., 2007; Hall, 2002; MacFarlane and Burchett, 2002). For
242 those metals (e.g., Pb) that are not essential nutrients for the plant growth, the defensive nature of
243 the plants will not actively translocate these metals to the root vascular tissues in a large quantity
244 (Lyubenova et al., 2013; Verbruggen et al., 2009). Therefore, the differences found in this study
245 reflect the nature of these metals as essential or non-essential nutrients for the plants and the
246 metal uptake mechanisms and transport pathways can be metal-dependent (Cheng, 2003; Lasat,
247 2002).
248
249 *2.3 Correlation analysis of metals in roots*

Table 2 shows the results of Pearson correlation analysis of the metal (Fe, Mn, Cu, Pb and Zn) concentrations in the epidermis and vascular tissue in each root sample. At Site TP-1, metals (Fe, Mn, Cu, Pb and Zn) in *Phragmites australis* and *Typha latifolia* show significant correlations in the epidermis ($p<0.05$), but no such significant correlation found in the vascular tissue ($p>0.05$). At Site TP-43, metals (Fe, Mn, Cu, Pb and Zn) in *Phragmites australis* roots also show significant correlations ($p<0.05$) in the epidermis. In the vascular tissue, Cu and Zn show significant correlations ($p<0.05$) with Fe. In addition, Cu also shows significant correlations with Mn and Zn (Table 2).

In the rhizosphere, the role of Fe plaque, which forms on the surface of plant roots, in regulating metal cycle has been an issue of much debate. Several studies suggest that the Fe plaque on the surface of roots serves as a barrier preventing heavy metals from entering plant roots (St-Cyr and Campbell, 1996; Sundby et al., 1998). However, others suggest that Fe plaque is not the main barrier (Ye et al., 1998; Liu et al., 2004). Understanding the function of Fe oxides in controlling the mobility of metals in plants is important in phytoextraction of metals from the contaminated soils (Tripathi et al., 2014). In this study, a strong association of metals (Cu, Mn, Pb and Zn) with Fe was found in the root epidermis (Figures 7-9). This could be a consequence of metal scavenges by Fe plaque or formation of Fe-Mn oxides (Bargar et al., 1997; Eick et al., 1999; Hansel et al., 2001; Ye et al., 1998). There were no such relationships found in the vascular tissue. The results suggest that, after the metal uptake by the plants from the soil, transport of metals from the epidermis to the vascular tissue, and accumulation in the root system can vary from metal to metal, most likely due to differential expression of a number of different accumulation systems with distinct metal-affinity patterns (Assunção et al., 2008). Some metals

may share the same transport pathways while others may not. The results from this study suggest that Fe-Mn oxides or Fe plaque appeared to play a role in governing the metal uptake at root-soil interface and metal transport and accumulation in the epidermis. Because of the high adsorption capacity of Fe-oxides, Fe plaque can be considered as a reactive substrate for metal sequestration (Feng et al., 2013; Hansel et al., 2001, 2002; Otte et al., 1989, 1991; Sundby et al., 1998; St-Cyr and Crowder, 1990, 1996). Although Fe oxide species vary in their formation pathways and activities towards metals, our results demonstrate that the root epidermis in *Typha latifolia* and *Phragmites australis* is an area of forming Fe plaque that can scavenge other metals such as Cu, Pb and Zn.

2.4 Factors governing metal transport and distributions in roots

Factor analysis was performed on metal (Cu, Fe, Mn, Pb and Zn) data to examine the factors governing the metal accumulation and distribution in the plant roots (Gotelli and Ellison, 2004). All the plants were analyzed together with separation of metal concentrations in the epidermis from that in the vascular tissue. For the epidermis, there are two factors which have eigenvalue greater than 0.5 and account for 77% of the total variance (Table 3). Factor 1 with high loadings of Zn (0.892) and Cu (0.884) and a moderate loading of Fe (0.647) explains 40% of the variation. This factor reflects the association of Zn and Cu with Fe in the epidermis of the plants, implying the adsorption of Cu and Zn on Fe oxides. In another words, a certain amount of Zn and Cu could be scavenged by Fe plaque in the epidermis during the transport. Factor 2 has high loadings of Mn (0.890) and Pb (0.883) and a moderate loading of Fe (0.521), and accounts for 37% of the variation (Table 3). This factor suggests that, as a non-essential

296 nutrient, Pb uptake, transport and accumulation in the epidermis are different from the other
297 nutrient metals (e.g., Cu and Zn) and can be controlled by Fe-Mn oxides (Feng et al., 2013;
298 Hansel et al., 2001, 2002). In the vascular tissue, the first three factors with eigenvalue greater
299 than 0.5 account for 86% of the total variance (Table 3). Individually, Factor 1 has a high loading
300 of Fe (0.923), a moderate loading of Zn (0.622) and a negative moderate loading of Mn (-0.642)
301 (Table 3). This factor is mainly an Fe factor and suggests that Fe and Zn may share some similar
302 mechanisms and pathways in the vascular tissue, but the mechanism is exclusive to Mn to a
303 certain extent. Factors 2, which accounts for 22% of the variation, has a high negative loading
304 of Pb (-0.960) and is essentially a Pb factor, suggesting that transport of Pb into the vascular
305 tissue is different from the other metals and this factor plays a negative role in the transport
306 (Table 3). Factor 3 is characterized by a high loading of Cu (0.925), a moderate loading of Zn
307 (0.589) and a negative moderate loading of Mn (-0.511), and explains 30% of the total variance
308 (Table 3). This factor suggests that Cu and Zn may share the same mechanism in transport into
309 the vascular tissue as nutrients required by the plants. In the meantime, the same mechanism
310 plays a moderate negative role in transporting Mn. This analysis suggests that although Cu, Zn
311 and Mn are essential nutrients for plant growth, the transport mechanisms are different. Overall,
312 the results indicate that the mechanisms controlling metal transport from the epidermis to the
313 vascular tissue can be very different and governed by individual factors or transport proteins
314 specifically for an individual metal.
315
316 **3. Conclusion**
317 This study demonstrates that synchrotron X-ray microbeam techniques have important
318 applications in studying metal spatial distributions in *Phragmites australis* and *Typha latifolia*

with a micro-scale resolution. Application of such state-of-the-art technologies can result in high-resolution information on spatial distribution of metals on wetland plants and their association with Fe plaque with very high sensitivity. The results from this study indicate that metal transport from the epidermis to the vascular bundle and metal distributions in the root tissues differ significantly, which depend on the metals and the plant species. As essential nutrients for plant growth, Cu and Zn are actively taken up by the roots and may share same transport pathways and similar mechanisms. Iron (Fe) and Mn, besides acting as essential nutrients for the plants, can form Fe plaque and Fe-Mn oxides that plays a major role in governing other metal transport in the plants by scavenging the other metals in the epidermis. In this study, *Phragmites australis* and *Typha latifolia* showed concentration dependent, metal preference patterns with regard metal accumulation, most likely due to differential expression of different uptake and transport systems with distinct metal-affinity patterns. As a result of the complex biogeochemical process, this study suggests that uptake of metals by the plant root system, or stabilization of metals within the plants provides a potential approach for brownfield remediation and wetland rehabilitation. Therefore, the results from this research will allow us to make broad inferences about the relevant plant uptake mechanisms. In other words, the sequestration of metal contaminants in the wetland plant root system suggests a potential low-cost remediation method (phytostabilization) to manage metal-contaminated sediments for brownfield remediation while performing wetland rehabilitation.

Acknowledgements

This work was supported in part by the Margaret and Herman Sokol Foundation (HF), China Scholarship Council (YQ) and the State Key Laboratory of Estuarine and Coastal

342 Research Open Research Fund (Ref #: SKLEC-KF201304) (HF, WZ, LY, YQ). This project was
343 also supported in part by the U.S. Department of Energy, Office of Science, Office of Workforce
344 Development for Teachers and Scientists (WDTS) under the Visiting Faculty Program (VFP)
345 (HF). Portions of this work were performed at Beamline X27A, National Synchrotron Light
346 Source (NSLS), and Biosciences Department, Brookhaven National Laboratory. Work in
347 Bioscience Department, BNL, was partially supported by the Division of Chemical Sciences,
348 Geosciences, and Biosciences, Office of Basic Energy Sciences of the US Department of Energy
349 through Grant DEAC0298CH10886 and the National Science Foundation through grant MCB-
350 1051675 (CJL). X27A is supported in part by the U.S. Department of Energy - Geosciences (DE-
351 FG02-92ER14244 to The University of Chicago - CARS). Use of the NSLS was supported by
352 the U.S. Department of Energy, Office of Science, Office of Basic Energy Sciences, under
353 Contract No. DE-AC02-98CH10886. We are also grateful to two anonymous reviewers who
354 offered constructive comments and suggestions on an earlier draft of this paper.
355

REFERENCES

Ablett, J.M., Kao, C.C., Reeder, R.J., Tang, Y., Lanzirotti, A., 2006. X27A—A new hard X-ray micro-spectroscopy facility at the National Synchrotron Light Source. Nucl. Instrum. Methods. Phys. Res. Sect. A 562, 487–494.

Assunção, A.G.L., Bleeker, P., ten Bookum, W.M., Vooijs, R., Schat, H., 2008. Intraspecific variation of metal preference patterns for hyperaccumulation in *Thlaspi caerulescens*: evidence for binary metal exposures. Plant Soil 303, 289–299.

Bargar, J.R., Persson, P., Brown, Jr. G.E., 1997. XAFS studies of Pb(II)-chloro and Hg(II)-chloro ternary complexes on goethite. J. Phys. IV France C2, 825-826.

Baxter, I.R., Vitek, O., Lahner, B., Muthukumar, B., Borghi, M., Morrissey, J., Guerinot, M.L., Salt, D.E., 2008. The leaf ionome as a multivariable system to detect a plant's physiological status. Proc. Natl. Acad. Sci. USA 105, 12081–12086.

Brune, A., Urbach, W., Dietz, K.J., 1994. Compartmentation and transport of Zn in barley primary leaves as basic mechanisms involved in Zn tolerance. Plant Cell Environ. 17, 153-162.

Cheng, S., 2003. Heavy metals in plants and phytoremediation. Environ. Sci. Pollut. Res. 10, 335-340.

Deng, D.M., Shu, W.S., Zhang, J., Zou, H.L., Lin, Z., Ye, Z.H., Wong, M.H., 2007. Zinc and cadmium accumulation and tolerance in populations of *Sedum alfredii*. Environ. Pollut. 147, 381-386.

Dzantor, E.K., Beauchamp, R.G., 2002. Phytoremediation, Part I: fundamental basis for the use of plants in remediation of organic and metal contamination. Environ. Prac. 4, 77-87.

379 Eick, M., Peak, J.D., Brady, P.V., Pesek, J.D., 1999. Kinetics of lead adsorption/desorption on
380 goethite: residence time effect. Soil Sci. 164(1), 28-39.
381 Feng, H., Cochran, J.K., Lwiza, H., Brownawell, B.J., Hirschberg, D.J., 1998. Distribution of
382 heavy metal and PCB contaminants in the sediments of an urban estuary: the Hudson River.
383 Mar. Environ. Res. 45, 69-88.
384 Feng, H., Han, X., Zhang, W., Yu, L., 2004. A preliminary study of heavy metal contamination
385 in Yangtze River intertidal zone due to urbanization. Mar. Pollut. Bull. 49, 910-915.
386 Feng, H., Yu, L., Solecki, W., 2005. Urban Dimensions of Environmental Change - Sciene,
387 Exposure, Policies, and Technologies. Science Press, Monmouth Junction, New Jersey.
388 Feng, H., Qian, Y., Gallagher, F.J., Wu, M., Zhang, W., Yu, L., Zhu, Q., Zhang, K., Liu, C.-J.,
389 Tappero, R., 2013. Lead accumulation and association with Fe on *Typha latifolia* root from
390 an urban brownfield site. Environ. Sci. Pollut. Res. 20, 3743-3750.
391 Gallagher, F.J., Pechmann, I., Bogden, J.D., Grabosky, J., Weis, P., 2008. Soil metal
392 concentrations and vegetative assemblage structure in an urban brownfield. Environ. Pollut.
393 153, 351-361.
394 Gilbert, B., Frenzel, P., 1998. Rice roots and CH_4 oxidation: the activity of bacteria, their
395 distribution and the microenvironment. Soil Biol. Biochem. 30, 1903-1916.
396 Gotelli, N.J., Ellison, A.M., 2004. A Primer of Ecological Statistics, first ed. Sinauer Associates,
397 Sunderland, MA, USA; p. 492.
398 Hall, J.L., 2002. Cellular mechanisms for heavy metal detoxification and tolerance. J. Exp. Bot.
399 53, 1-11.

400 Hansel, C.M., Fendorf, S., Sutton, S., Newville, M., 2001. Characterization of Fe plaque and
401 associated metals on the roots of mine-waste impacted aquatic plants. Environ. Sci. Technol.
402 35, 3863-3868.
403 Hansel, C.M., Laforce, M.J., Fendorf, S., Sutton, S., 2002. Spatial and temporal association of
404 As and Fe species on aquatic plant roots. Environ. Sci. Technol. 36, 1988-1994.
405 Hinsinger, P., Courchesne, F., 2008. Biogeochemistry of metals and metalloids at the soil–root
406 interface. A. Violante, P.M. Huang, G.M. Gadd (Eds.), Biophysico-chemical Processes of
407 Heavy Metals and Metalloids in Soil Environments, Wiley-Interscience, Hoboken, NJ, pp.
408 268-311
409 Jones, K.W., Wang, J., Chen, Y., Yuan, Q., Lindquist, W.B., Beckingham, L., Peters, C.A., Um,
410 W., Newman, L., Sabo-Attwood, T., Tappero, R., 2013. Tomographic investigations relevant
411 to the rhizosphere In: Anderson SH and Hopmans JW, editors. Soil–Water–Root Processes:
412 Advances in Tomography and Imaging. SSSA Special Publication 61. Madison, Wisconsin;
413 p. 23-39.
414 Koelmel, J., Amarasiriwardena, D., 2012. Imaging of metal bioaccumulation in Hay-scented fern
415 (*Dennstaedtia punctilobul*a) rhizomes growing on contaminated soils by laser ablation ICP-
416 MS. Environ. Pollut. 168, 62-70.
417 Lacerda, L.D., Freixo, J.L., Coelho, S.M., 1997. The effect of *Spartina alterniflora* Loisel on
418 trace metals accumulation in inter-tidal sediments. Mangroves Salt Marshes 1, 201-209.
419 Lasat, M.M., 2002. Phytoextraction of toxic metals: a review of biological mechanisms. J.
420 Environ. Qual. 31, 109-120.
421 Liberty State Park (LSP), 2008. Liberty State Park Interpretive Plan.

422 Liu, W.-J., Zhu, Y.-G., Smith, F.A., Smith, S.E., 2004. Do iron plaque and genotypes affect
423 arsenate uptake and translocation by rice seedlings (*Oryza sativa* L.) grown in solution
424 culture? J. Exp. Bot. 55, 1707-1713.
425 Lyubenova, L., Pongrac, P., Vogel-Mikuš, K., Mezek, G.K., Vavpetiič, P., Grlj, N., Regvar, M.,
426 Pelicon, P., Schröder, P., 2013. The fate of arsenic, cadmium and lead in Typha latifolia: A
427 case study on the applicability of micro-PIXE in plant ionomics. J. Hazard. Mater. 248, 371-
428 378.
429 MacFarlane, G.R., Burchett, M.D., 2002. Toxicity, growth and accumulation relationships of
430 copper, lead and zinc in the grey mangrove, *Avicennia marina* (Forsk.) Vierh. Mar. Environ.
431 Res. 54, 65-84.
432 Marschner, P., 2012. Marschner's Mineral Nutrition of Higher Plants (P. Marschner Ed. 3rd ed.).
433 USA: Academic Press.
434 Martin, R.R., Naftel, S.J., Skinner, W., Jones, K.W., Feng, H., 2003. Micro-synchrotron x-ray
435 fluorescence of the metal distribution in a black spruce tree stem: evidence from radial
436 mobility. X-Ray Spectrom. 32, 402-407.
437 Martin, R., Naftel, S., Macfie, S., Jones, K., Feng, H., Trembley, C., 2006. High variability of the
438 metal content of tree growth rings as measured by synchrotron micro x-ray fluorescence
439 spectrometry. X-Ray Spectrom. 35, 57-62.
440 McLaughlin. M.J., Smolders, E., Merckx, R.,1998. Soil-root interface: physiochemcial processes.
441 Soil Sci. Eco. Health. 52, 233-277.
442 Merchant, S.S., 2010. The elements of plant micronutrients. Plant Physiol. 154, 512-515.
443 Morrissey, J., Guerinot, M., 2009. Iron uptake and transport in plants: the good, the bad, and the
444 ionome. Chem. Rev. 109, 4553-4567.

445 Naftel, S.J., Martin, R.R., Jones, K.W., Feng, H., Savard, M.M., Bégin, C., 2001. Synchrotron
446 radiation analysis of a smelter impacted tree-ring sample. Can. J. Anal. Sci. Spect. 46(4),
447 118-122.
448 N.J.D.E.P. (New Jersey Department of Environmental Protection), 1995. Liberty State Park Site
449 Status Report.
450 Otte, M.L., Rozema, J., Koster, L., Haarsma, M.S., Broekman, R.A., 1989. Iron plaque on roots
451 of *Aster tripolium* L.: interaction with zinc uptake. New Phytol 111, 309-317.
452 Otte, M.L., Dekkers, I.M.J., Rozema, J., Broekman, R.A., 1991. Uptake of arsenic by *Aster*
453 *tripolium* in relation to rhizosphere oxidation. Can. J. Botany 69(12), 2670-2677.
454 Palmer, C.M., Guerinot, M.L., 2009. Facing the challenges of Cu, Fe and Zn homeostasis in
455 plants. Nat. Chem. Biol. 5, 333-340.
456 Punshon, T., Guerinot, M., Lanzirotti, A., 2009. Using synchrotron X-ray fluorescence
457 microprobes in the study of metal homeostasis in plants. Ann. Bot. 103, 665-672.
458 Qian, Y., Gallagher, F.J., Feng, H., Wu, M., 2012. A geochemical study of toxic metal
459 translocation in an urban brownfield wetland. Environ. Pollut. 166, 23-30.
460 Qian, Y., 2015. Biogeochemical Studies of Metal Uptake and Transportation in Plants on an
461 Urban Brownfield. Dissertation, Montclair State University.
462 Rascio, N., Navari-Izzo, F., 2011. Heavy metal hyperaccumulating plants: how and why do they
463 do it? And what makes them so interesting? Plant Sci. 180(2), 169-181.
464 St-Cyr, L., Crowder, A.A., 1990. Manganese and copper in the root plaque of *Phragmites*
465 *australis* (Cav.) Trin. ex Steudel. Soil Sci. 149, 191-198.

466 St-Cyr, L., Campbell, P.G.C., 1996. Metals (Fe, Mn, Zn) in the root plaque of submerged aquatic
467 plants collected in situ: Relations with metal concentrations in the adjacent sediments and in
468 the root tissue. Biogeochemistry 33, 45-76.
469 Sundby, B., Vale, C., Caçador, I., Catarino, F., Madureira, M.J., Caetano, M., 1998. Metal-rich
470 concretions on the roots of salt marsh plants: mechanism and rate of formation. Limnol.
471 Oceanogr. 43, 245-252.
472 Taiz, L., Zeiger, E., 2006. Plant physiology. Sunderland, M.A: Sinaur Associates Inc.
473 Tripathi, R.D., Tripathi, P., Dwivedi, S., Kumar, A., Mishra, A., Chauhan, P.S., Norton, G.J.,
474 Nautiyal, C.S., 2014. Roles for root iron plaque in sequestration and uptake of heavy metals
475 and metalloids in aquatic and wetland plants. Metallomics 6, 1789-1800.
476 United States Army Corps of Engineers (USACE), 2005. Hudson-Raritan Estuary Environmental
477 Restoration Study, Liberty State Park, Environmental Resource Inventory.
478 Verbruggen, N., Hermans, C., Schat, H., 2009. Molecular mechanisms of metal
479 hyperaccumulation in plants, New Phytol. 181, 759-776.
480 Weis, J.S., Weis, P., 2004. Metal uptake, transport and release by wetland plants: implications
481 for phytoremediation and restoration. Environ. Inter. 30, 685-700.
482 Williams, T.P., Bubb, J.M., Lester, J.N., 1994. Metal accumulation within salt marsh
483 environments: A review. Marine, Pollut. Bull. 28, 273-290.
484 Ye, Z.H., Baker, A.J.M., Wong, M.H., Willis, A.J., 1998. Zinc, lead and cadmium accumulation
485 and tolerance in *Typha latifolia* as affected by iron plaque on the root surface. Aquat. Bot. 61,
486 55–67.

487 Zhang, W., Feng, H., Chang, J., Qu, J., Xie, H., Yu, L., 2009. Heavy metal contamination in
488 surface sediments of Yangtze River intertidal zone: an assessment from different indexes.
489 Environ. Pollut. 157, 1533-1543.
490

491 **Figure caption**

492

493 Figure 1. Map showing the study area in Liberty State Park. Sites TP-1 and TP-43 were
494 selected for this study. The vegetation assembling patterns: SNH, successional northern
495 hardwood; SSB, successional shrubland; SOF, successional old field; MS, maritime shrubland;
496 MG, maritime grasslands; CRM, common reed/mugwort; FFW, floodplain forested wetlands;
497 SSW, shrub swamp wetland; SEM, shallow emergent marsh; CRW, common-reed-dominated
498 wetland.

499 Figure 2. Three-dimensional tomographic root structure images of *Typha latifolia* and
500 *Phragmites australis* from synchrotron μCMT measurement. Upper panel: synchrotron X-ray
501 images of the original roots in Kapton tubes. Lower panel: reconstructed root images from
502 synchrotron μCMT measurement. The samples were collected at Site TP-1 in May 2011.

503 Figure 3. Cross-section images of the plant root tissue from synchrotron μCMT measurement for
504 a) *Typha latifolia* root, and b) *Phragmites australis* root. It is seen that high X-ray attenuation
505 occurs in epidermis associated with the root tissue structure. Pixel size is 4 μm. The samples
506 were collected at Site TP-1 in May 2011.

507 Figure 4. Two-dimensional (2D) maps show the information of a cross-section of *Phragmites*
508 *australis* root sample collected at Site TP-1 in September 2011. Optical image shows the root
509 tissue structures of *Phragmites australis*. The framed areas in epidermis and vascular tissue of
510 *Phragmites australis* root thin section (30 μm in thickness) were selected for statistical analysis.
511 Images from synchrotron radiation measurement show Cu, Fe, Mn, Pb and Zn concentrations
512 and distributions in the root tissue.

Figure 5. Two-dimensional (2D) maps show the information of a cross-section of *Typha latifolia* root sample collected at Site TP-1 in May 2011. Optical image shows the root tissue structures of *Typha latifolia*. The framed areas in epidermis and vascular tissue of *Typha latifolia* root thin section (30 μm in thickness) were selected for statistical analysis. Images from synchrotron radiation measurement show Cu, Fe, Mn, Pb and Zn concentrations and distributions in the root tissue.

Figure 6. Two-dimensional (2D) maps show the information of a cross-section of *Phragmites australis* root sample collected at Site TP-43 in May 2011. Optical image shows the root tissue structures of *Phragmites australis*. The framed areas in epidermis and vascular tissue of *Phragmites australis* root thin section (30 μm in thickness) were selected for statistical analysis. Images from synchrotron radiation measurement show Cu, Fe, Mn, Pb and Zn concentrations and distributions in the root tissue.

Figure 7. Relationship of Cu, Mn, Pb and Zn with Fe in the epidermis of *Typha latifolia* root collected at Site TP-1 in May 2011. Significant correlation between metals (Cu, Mn, Pb and Zn) and Fe indicates metal scavenge by Fe plaque and formation of Fe-Mn oxides.

Figure 8. Relationship of Cu, Mn, Pb and Zn with Fe in the epidermis of *Phragmites australis* root collected at Site TP-1 in September 2011. Significant correlation between metals (Cu, Mn, Pb and Zn) and Fe indicates metal scavenge by Fe plaque and formation of Fe-Mn oxides.

534 Figure 9. Relationship of Cu, Mn, Pb and Zn with Fe in the epidermis of *Phragmites australis*
535 root collected at Site TP-43 in May 2011. Significant correlation between metals (Cu, Mn, Pb
536 and Zn) and Fe indicates metal scavenge by Fe plaque and formation of Fe-Mn oxides.

Figure1

Click here to download high resolution image

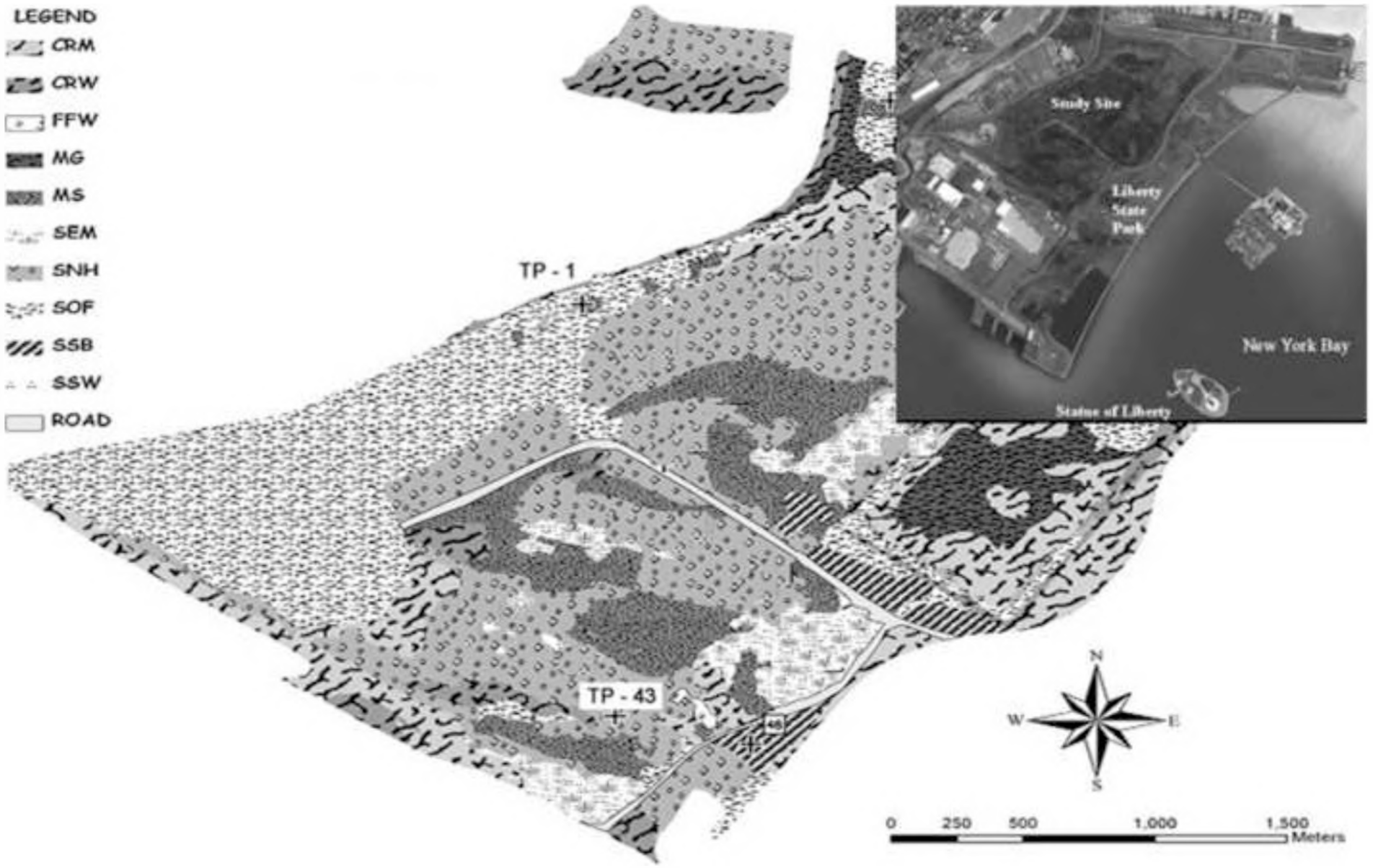

Figure2
Click here to download high resolution image

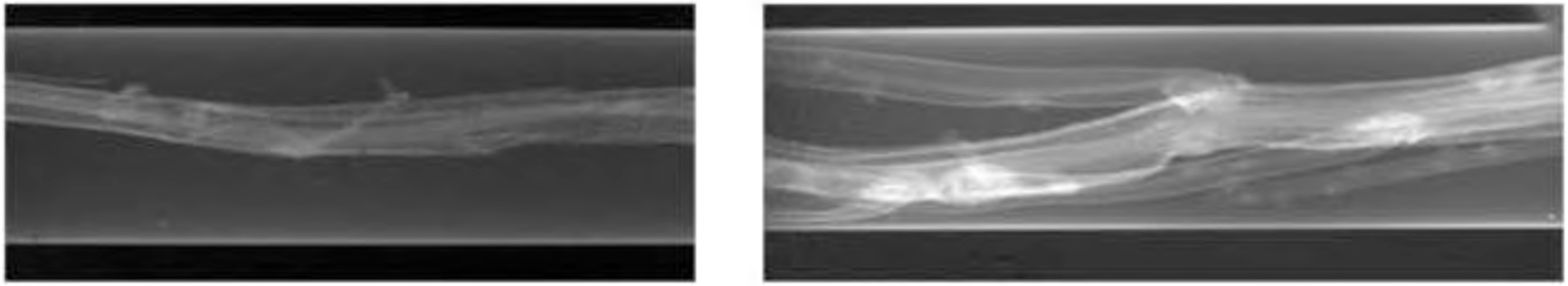

Synchrotron X-ray image

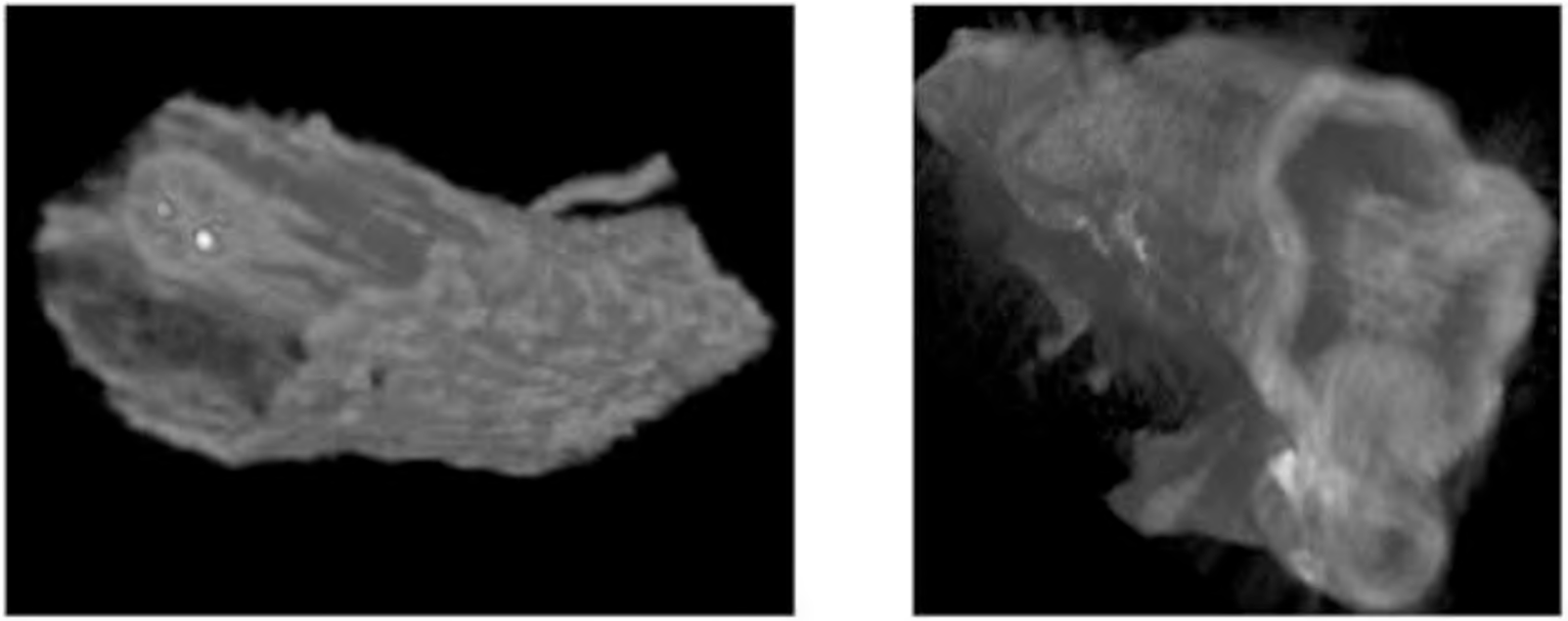

Reconstructed image

a. *Typha latifolia*

b. *Phragmites australis*

Figure3
Click here to download high resolution image

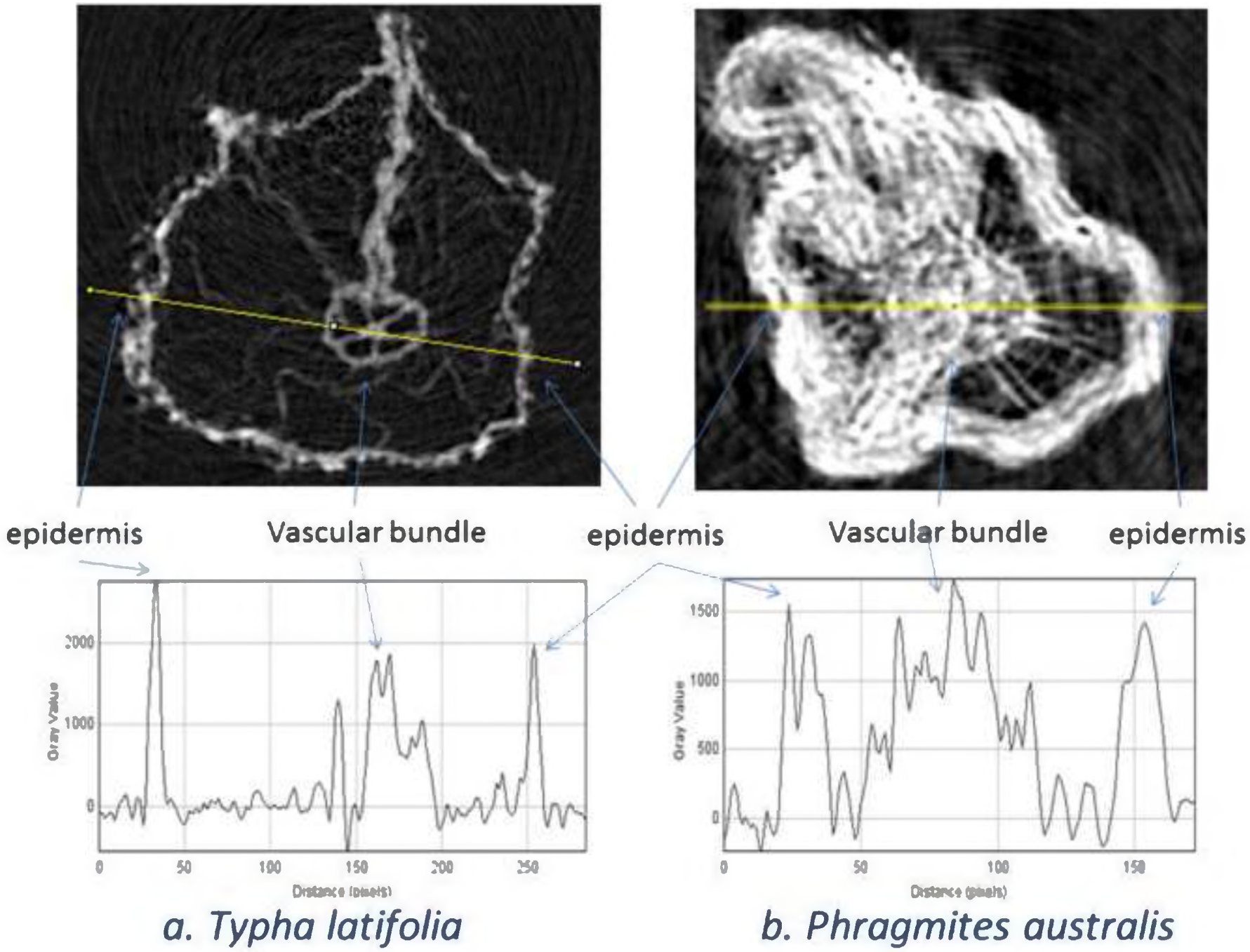

a. Typha latifolia

b. Phragmites australis

Figure4

Click here to download high resolution image

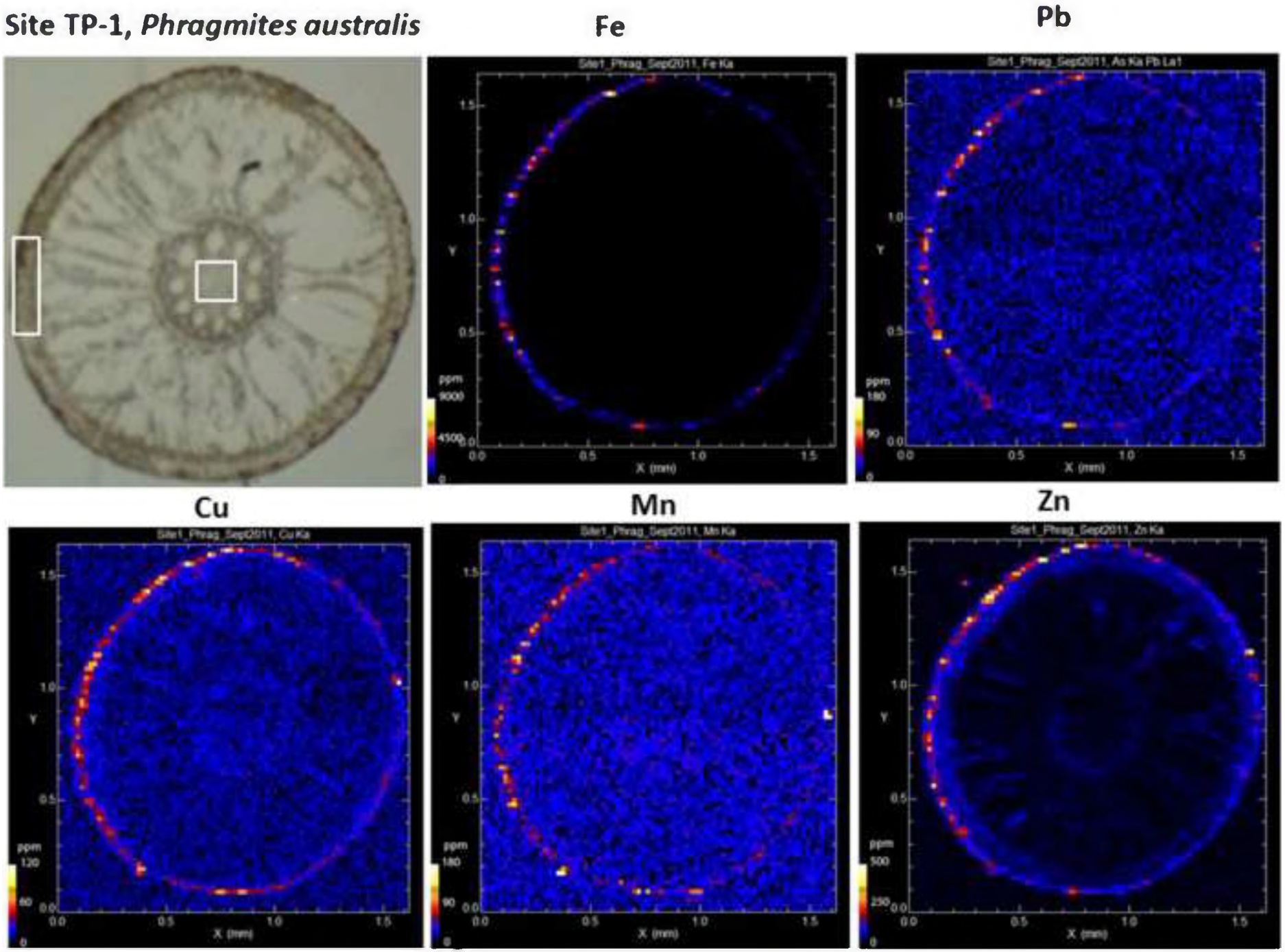

Figure5

Click here to download high resolution image

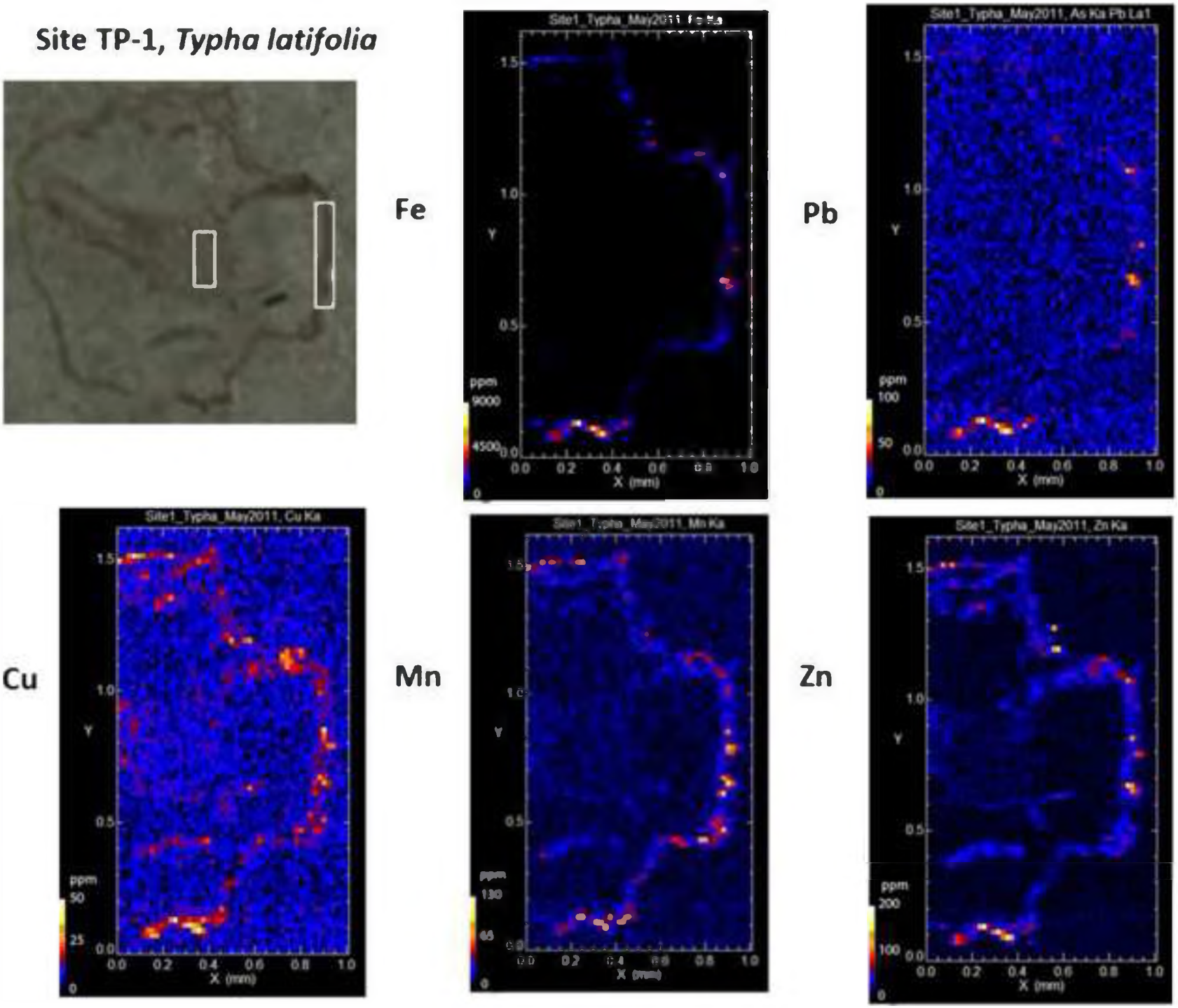

Figure6

Click here to download high resolution image

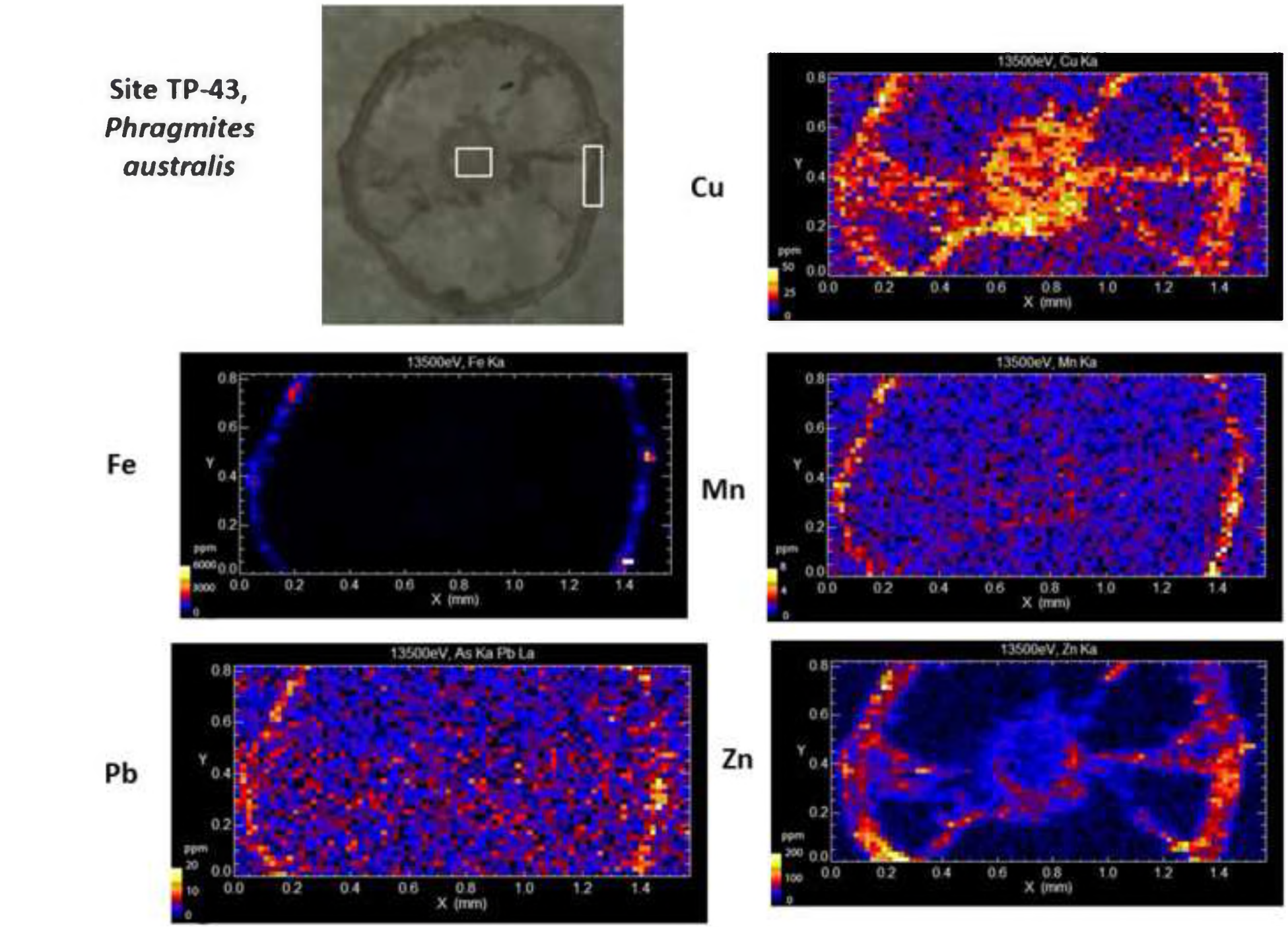

Figure7

Click here to download high resolution image

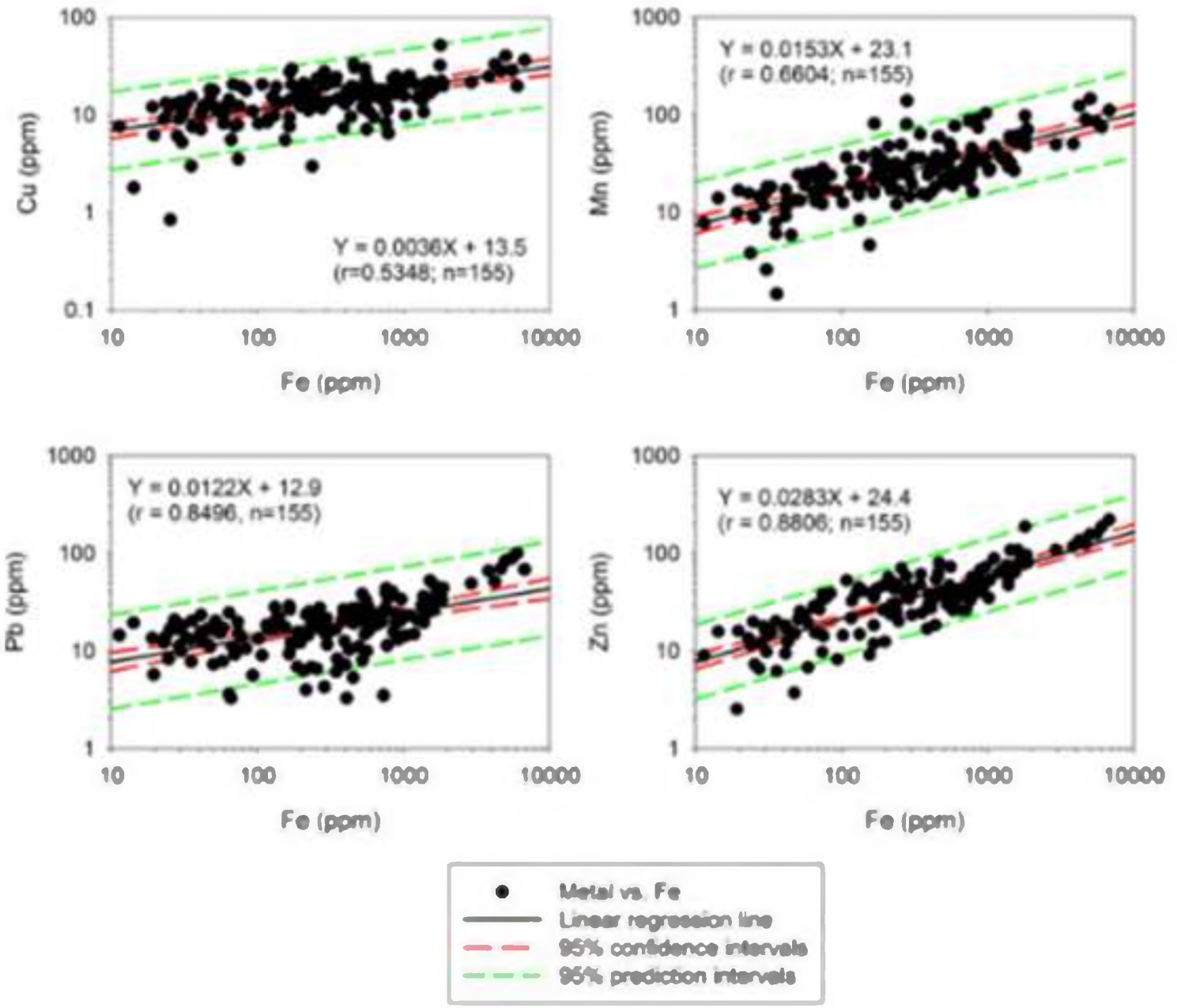

Figure8

Click here to download high resolution image

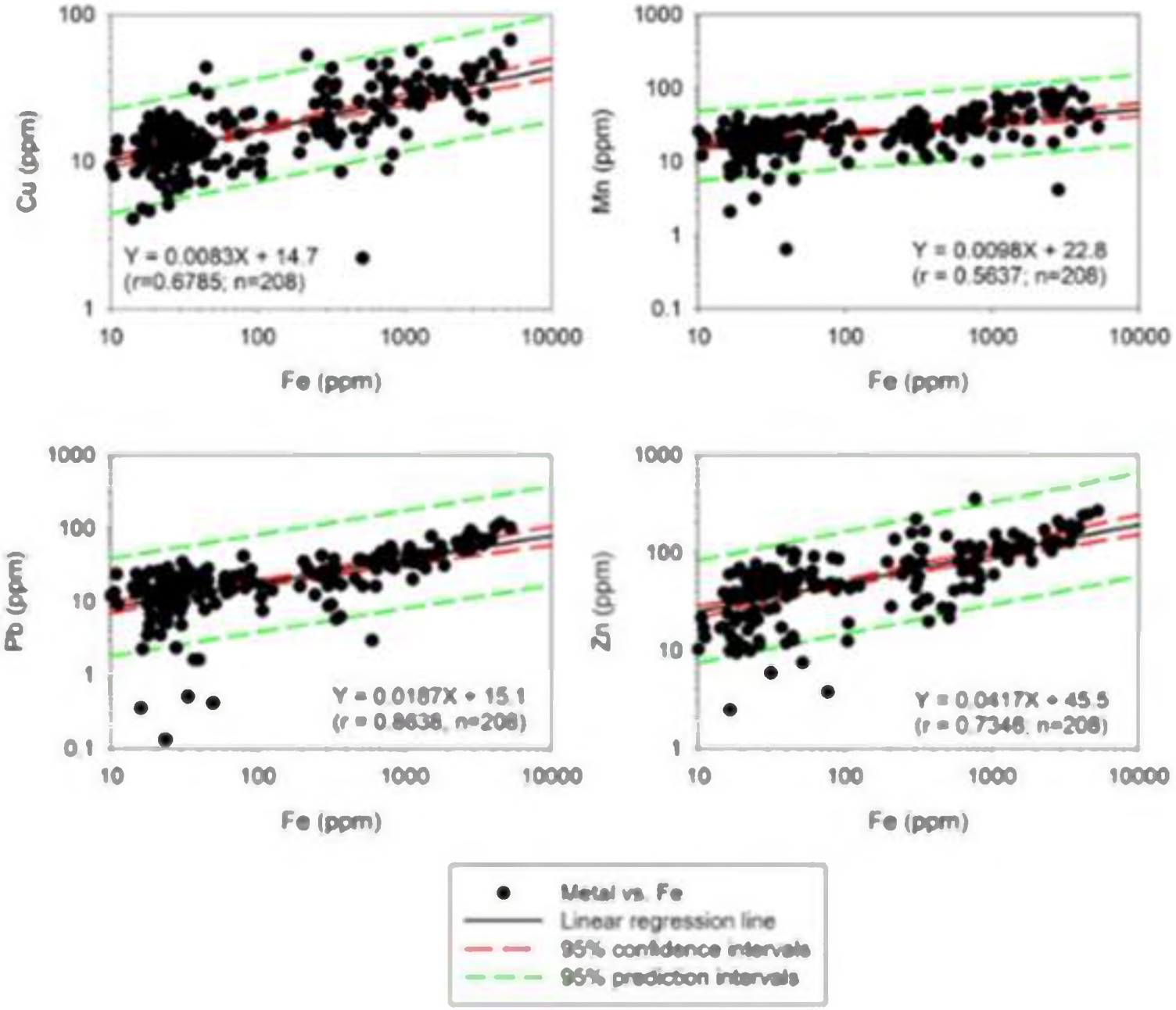

Figure9

Click here to download high resolution image

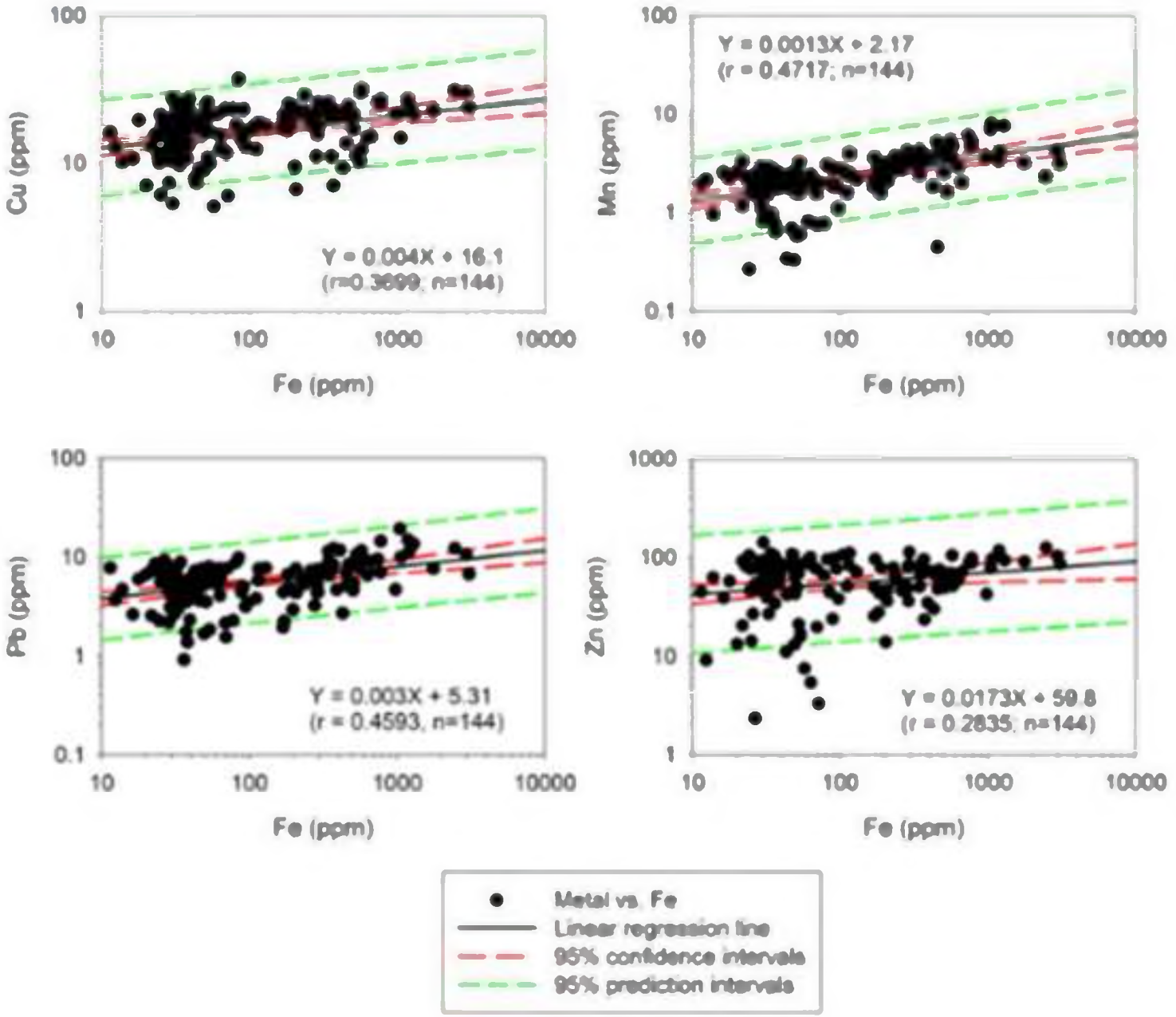

Table1
Click here to download high resolution image

Table 1

Average concentrations ($\mu g\ g^{-1}$) of Cu, Fe, Mn, Pb and Zn in the representatives areas within the epidermis (E) and vascular tissue(V) of *Phragmites australis* and *Typha latifolia* roots collected at Sites TP-1 and TP-43, respectively. Statistical analysis shows significant difference ($p<0.01$) in the concentrations between epidermis and vascular tissue.

Site	Species	Sample size (n)	Element	Epidermis mean ± s.d.	Vascular bundle mean ± s.d.	*p* value
Site TP-1	*P. australis*	E = 208	Fe	474 ± 913	19.3 ± 5.2	0.000
		V = 81	Mn	27.4 ± 15.9	20.5 ± 8.9	0.000
			Cu	18.7 ± 11.2	10.0 ± 3.6	0.000
			Pb	23.9 ± 19.8	14.2 ± 7.4	0.000
			Zn	65.2 ± 51.8	11.0 ± 4.4	0.000
	T. latifolia	E = 155	Fe	686 ± 1120	25.0 ± 7.2	0.000
		V = 110	Mn	33.6 ± 26.0	11.2 ± 4.5	0.000
			Cu	16.0 ± 7.5	9.35 ± 3.44	0.000
			Pb	21.3 ± 16.1	12.6 ± 6.9	0.000
			Zn	43.9 ± 36.1	13.9 ± 4.9	0.000
Site TP-43	*P. australis*	E = 144	Fe	265 ± 479	36.5 ± 9.1	0.000
		V = 120	Mn	2.51 ± 1.33	1.88 ± 0.76	0.000
			Cu	17.4 ± 6.4	20.6 ± 5.6	0.000
			Pb	6.09 ± 3.09	4.91 ± 2.29	0.001
			Zn	64.4 ± 29.2	39.2 ± 15.8	0.000

Table2

Click here to download high resolution image

Table 2

Results of Pearson correlation between metals in epidermis (E) and vascular tissue (V), respectively. Bold face indicates a significant correlation level at 5% two-tailed significance.

Site	Species	Sample size (n)	Epidermis (E)						Vascular bundle (VB)				
				Fe	Mn	Cu	Pb	Zn	Fe	Mn	Cu	Pb	Zn
Site TP-1	*P. australis*	E = 208	Fe	1.000					1.000				
		V = 81	Mn	**0.564**	1.000				-0.010	1.000			
			Cu	**0.678**	**0.465**	1.000			0.036	0.022	1.000		
			Pb	**0.864**	**0.574**	**0.655**	1.000		0.004	0.109	-0.022	1.000	
			Zn	**0.735**	**0.460**	**0.810**	**0.706**	1.000	0.106	0.169	0.168	0.146	1.000
	T. latifolia	E = 155	Fe	1.000					1.000				
		V = 110	Mn	**0.660**	1.000				-0.038	1.000			
			Cu	**0.535**	**0.694**	1.000			-0.019	0.147	1.000		
			Pb	**0.850**	**0.595**	**0.426**	1.000		0.115	**-0.298**	0.019	1.000	
			Zn	**0.881**	**0.756**	**0.721**	**0.723**	1.000	0.181	0.029	0.004	0.186	1.000
Site TP-43	*P. australis*	E = 144	Fe	1.000					1.000				
		V = 120	Mn	**0.472**	1.000				0.011	1.000			
			Cu	**0.370**	**0.263**	1.000			**0.195**	**0.186**	1.000		
			Pb	**0.459**	**0.457**	**0.227**	1.000		-0.035	-0.066	0.038	1.000	
			Zn	**0.284**	**0.256**	**0.466**	**0.227**	1.000	**0.387**	0.048	**0.550**	-0.093	1.000

Table3

Click here to download high resolution image

Table 3.

Results of factor analysis. Eigenvalue is set at 0.5 as a cut off value.

Epidermis

Latent Roots (Eigenvalues)

1	2	3	4	5
2.598	1.283	0.444	0.36	0.315

Rotated Loading Matrix (VARIMAX, Gamma = 1.000000)

	1	2
log Zn	0.892	0.045
log Cu	0.884	0.100
log Fe	0.647	0.521
log Mn	0.044	0.890
log Pb	0.166	0.883

Percent of Total Variance Explained

1	2
40.497	37.113

Vascular tissue

Latent Roots (Eigenvalues)

1	2	3	4	5
3.019	0.684	0.615	0.386	0.296

Rotated Loading Matrix (VARIMAX, Gamma = 1.000000)

	1	2	3
log Fe	0.923	0.135	0.115
log Mn	-0.642	-0.3	-0.511
log Zn	0.622	0.189	0.589
log Pb	-0.195	-0.96	-0.189
log Cu	0.164	0.162	0.925

Percent of Total Variance Explained

1	2	3
34.299	21.827	30.249